ARTICLE
Journal of Cellular Biochemistry 114:2823–2833 (2013)

Journal of Cellular Biochemistry

The R740S Mutation in the V-ATPase a3 Subunit Results in Osteoclast Apoptosis and Defective Early-Stage Autophagy

Noelle Ochotny,[1] Irina Voronov,[1] Celeste Owen,[2] Jane E. Aubin,[1,2,3] and Morris F. Manolson[1*]

[1]*Faculty of Dentistry, Dental Research Institute, University of Toronto, Toronto, Ontario, Canada*

[2]*Centre for Modeling Human Disease, Samuel Lunenfeld Research Institute, Mt. Sinai Hospital, Toronto, Ontario, Canada*

[3]*Department of Molecular Genetics, University of Toronto, Toronto, Ontario, Canada*

ABSTRACT

Vacuolar-type H^+-ATPases (V-ATPases) are located in lysosomes and at the ruffled border in osteoclasts. We showed previously that the R740S mutation is dominant negative for V-ATPase activity, uncouples proton transport from ATP hydrolysis and causes osteopetrosis in heterozygous mice (+/R740S). Here we show mice homozygous for R740S (R740S/R740S) have more severe osteopetrosis and die by postnatal day 14. Although R740S/R740S osteoclasts express wild-type levels of a3, it is mislocalized. Acridine orange staining of R740S/R740S osteoclasts grown on a Corning resorptive surface reveals no resorption and no acidification of intracellular compartments. Whereas osteoblast and osteocyte apoptosis is normal, R740S/R740S osteoclasts exhibit increased apoptosis compared with wild-type osteoclasts. Localization of the enzyme tartrate-resistant acid phosphatase (TRAP) is also aberrant. Transmission electron microscopy reveals that R740S/R740S osteoclasts do not polarize, lack ruffled borders, and contain fewer autophagosomes. Consistent with an early stage defect in autophagy, expression of LC3II is reduced and expression of p62 is increased in R740S/R740S compared to wild-type osteoclasts. These results indicate the importance of intracellular acidification for the early stages of autophagy as well as for osteoclast survival, maturation, and polarization with appropriate cytoplasmic distribution of key osteoclast enzymes such as TRAP. J. Cell. Biochem. 114: 2823–2833, 2013.

KEY WORDS: VACUOLAR H^+-ATPASE; PROTON TRANSPORT; OSTEOCLAST; BONE BIOLOGY

Osteoclasts and osteoblasts are vital mediators of the tightly regulated bone remodeling process. Osteoblasts, of mesenchymal origin, are the bone-forming cells. Osteoclasts, of the hematopoietic lineage, are large, multinucleated cells found at the bone surface where they resorb bone. In order to resorb bone, osteoclasts adhere to the bone surface, become polarized, and form a tight seal (sealing zone) and a specialized membrane called the ruffled border. Into this sealed area, osteoclasts pump protons to acidify the surface mineral component of bone and then secrete enzymes to digest the extracellular matrix proteins. When the balance between bone formation and bone resorption is altered, the pathological result is that bone mass is either increased (osteopetrosis) or decreased (osteoporosis).

Osteopetrosis describes a heterogeneous group of diseases with varying degrees of osteoclast dysfunction. The most severe form of osteopetrosis is autosomal recessive infantile malignant osteopetrosis (ARO). Children with ARO have osteoclasts that are morphologically normal but are unable to resorb bone due to defects in the acidification of the space between the osteoclast and the bone surface [Frattini et al., 2000; Kornak et al., 2000, 2001; Chalhoub et al., 2003; Taranta et al., 2003]. The lack of resorption causes dense bone, bone marrow failure, anemia, and hepatosplenomegaly

Disclosure Statement: None.
Jane E. Aubin and Morris F. Manolson contributed equally to this work.
Grant sponsor: Canadian Institutes of Health Research; Grant numbers: FRN 69198, FRN MOP-79322; Grant sponsor: CIHR Strategic Training Program Cell Signaling in Mucosal Inflammation and Pain; Grant sponsor: Faculty of Dentistry (University of Toronto) Harron Fund.
*Correspondence to: Morris F. Manolson, Faculty of Dentistry, University of Toronto, 124 Edward St., Toronto, Ontario, Canada M5G 1G6. E-mail: m.manolson@utoronto.ca
Manuscript Received: 16 July 2013; Manuscript Accepted: 22 July 2013
Accepted manuscript online in Wiley Online Library (wileyonlinelibrary.com): 1 August 2013
DOI 10.1002/jcb.24630 • © 2013 Wiley Periodicals, Inc.

[Gerritsen et al., 1994; Fasth and Porras, 1999]. Over 50% of human cases of osteopetrosis are due to mutations in the a3 subunit of vacuolar-type H^+-ATPases (V-ATPase), the proton pump responsible for acidification of the bone surfaces [Kornak et al., 2000; Sobacchi et al., 2001; Frattini et al., 2003].

V-ATPases are ubiquitous multi-subunit enzymes that consist of a membrane-embedded proton translocation domain V_0, containing the a, c, c′, d, and e subunits, and a cytoplasmic ATP hydrolysis domain V_1, containing the A–H subunits [Nishi and Forgac, 2002; Kawasaki-Nishi et al., 2003; Toei et al., 2010]. The V_0 subunit 'a' has four isoforms, a1–a4. The a1 and a2 are ubiquitously expressed, while a4 is found in kidney, inner ear, and testes [Toyomura et al., 2003; Pietrement et al., 2006]. Although found in other cells, the a3 isoform is highly enriched in osteoclasts [Manolson et al., 2003], where it localizes to lysosomes and plasma membranes in non-resorbing osteoclasts and to the ruffled border in actively resorbing osteoclasts [Toyomura et al., 2003]. Beyond the association of a3 mutations with human osteopetrosis, the importance of this subunit is further demonstrated by the phenotype of mouse models: both the *oc*/*oc* mouse, a spontaneous mutation causing truncation of the N-terminal portion of a3 [Schlager and Dickie, 1967; Marks et al., 1985], and the *Tcirg1*$^{-/-}$ mouse [Li et al., 1999] do not express the a3 protein, have progressive osteopetrosis and die within 3–5 weeks. Although osteoclasts in both models appear morphologically normal, they do not acidify or resorb bone [Marks et al., 1985; Li et al., 1999].

We previously reported that a dominant negative missense mutation in a3 (*Arg740Ser* [R740S]) causes mild osteopetrosis in heterozygous mice (+/R740S) due to decreased bone resorption [Ochotny et al., 2011]. This mutation replaces the evolutionarily conserved arginine 740, involved in translocating protons across the membrane [Kawasaki-Nishi et al., 2001], with serine, abolishing proton pumping. Unlike osteoclasts from humans with a3 mutations, or mouse models that lack the a3 subunit, the +/R740S osteoclasts within long bones are polarized and form ruffled border membranes [Ochotny et al., 2011]. Here we show that osteoclasts from mice homozygous for the R740S mutation (R740S/R740S) do not polarize and lack ruffled border membranes, a feature similar to the *oc*/*oc* and *Tcirg1*$^{-/-}$ mouse models of osteopetrosis. At the same time, these cells display unique phenotypic traits not seen in these other models such as lack of intracellular acidification, increased osteoclast apoptosis and defective autophagy.

MATERIALS AND METHODS

MICE

Mice were generated as described by Ochotny et al. [2011]. Female and male +/R740S heterozygous mice were bred to produce homozygous R740S/R740S F1. All experimental procedures received approval from the local animal care committees and were conducted in accordance with the guidelines of the Canadian Council on Animal Care.

GENOTYPING

DNA was extracted from small pieces of tails incubated in 100 μl of PCR buffer containing 10× PCR buffer, 0.1 M DTT, 1 mg/ml proteinase K, and 10% SDS and incubated at 55°C for 2.5 h, then amplified with Primer 1 (TTGAGGGAAGGGAAGCACCTTT) and Primer 2 (TAAGAACGACCCACCCAACTCA). The PCR products were digested with Hinf1 (Invitrogen, Burlington, ON, Canada), separated on a 1.5% agarose gel and the genotype was determined based on the number and molecular weight of the bands: wild type, one band at 472 kb; heterozygote, three bands at 472, 304, and 167 kb; homozygote, two bands at 304 and 167 kb.

SERUM MEASUREMENTS

Serum was collected from 9- and 10-day-old mice (5 mice/genotype) and used to measure total calcium, total phosphate, and total glucose (IDEXX Laboratories, Burlington, ON, Canada).

BALANCE TESTS

The mice were tested individually. The righting reflex was tested by placing the mouse in the center of a horizontal metal pole that was gradually lifted to a vertical position. Normal mice will grip the pole and walk up and down the pole. The mice were then placed in an uncapped 50 ml Falcon tube with air holes drilled into the closed end, and the tube was turned sideways. Normal mice will move in the direction opposite to the turning. Next the mice were observed for 3 min in a viewing box where the gait and posture were observed. Three mice per genotype at P14 were analyzed.

HISTOPATHOLOGY

Histopathology was performed at the Centre for Modeling Human Disease, Samuel Lunenfeld Institute, affiliated with Mount Sinai Hospital in Toronto, ON, Canada. A total of 13 mice underwent histopathology that included P0, n = 3 mice/genotype and P14, n = 3 +/+ and n = 4 R740S/R740S.

MICRO-COMPUTED TOMOGRAPHY (μCT)

The left femurs were scanned with a GE Healthcare eXplore Locus SP instrument (Baie d'Urfe, Quebec, Canada). Two-dimensional images were used to generate 3D reconstructions of bones from n = 3 per genotype at P10. Morphometric parameters were calculated with 3D software eXplore Microview V.2.2 supplied with the instrument.

TRANSMISSION ELECTRON MICROSCOPE (TEM) IMAGING

Femurs from newborn mice (4 per genotype) were fixed and prepared for TEM as described previously [Ochotny et al., 2011]. Samples were viewed with a Hitachi H-7000 electron microscope (Toronto, ON, Canada) and a Hamamatsu ORCA-HR digital camera (Hammamitsu City, Japan) in the Microscope Imaging Laboratory (MIL) at the University of Toronto.

PARAFFIN EMBEDDED SPECIMENS

Femurs of mice at 1, 2, and 3 days of age (4 mice/genotype) were excised, cleaned of soft tissue, fixed, and decalcified in 1.9% gluteraldehyde and 0.15 M EDTA for 3 days, embedded in paraffin and sectioned at 5 μm thickness. Sections were stained with hematoxylin and eosin and for tartrate-resistant acid phosphatase (TRAP).

TUNEL STAINING

Unstained sections prepared as above were deparaffinized in xylenes, rehydrated in decreasing concentrations of ethanol, and used for

colorimetric detection of apoptotic cells with the fragEL DNA Fragmentation Kit according to the manufacturer's directions (Calbiochem, EMD Biosciences, Burlington, ON, Canada). The total number of osteoclasts, osteoblasts, and osteocytes and the number of cells with apoptotic nuclei were counted.

IMMUNOHISTOCHEMISTRY

Unstained sections prepared as above were deparaffinized in xylenes then rehydrated in decreasing concentrations of ethanol. The deparaffinized sections underwent antigen retrieval in either citrate buffer, pH 6.0 for the LC3 antibody (Thermo Scientific, Rockford, IL), or Tris–EDTA buffer, pH 9.0 overnight at 60°C for the Anti-SQSTM1/p62 antibody (Abcam, Cambridge, MA). No antigen retrieval was needed for the V-ATPase a3 (rabbit polyclonal antibody, custom made by Cedarlane Laboratories, Burlington, ON, Canada using RNTQRRRAGQQDEDTDKLLASPDASTLEN peptide). Immunochemical staining was performed using the Vectastain Elite ABC Kit (Vector Laboratories, Burlingame, CA) according to the manufacturer's instructions. Diaminobenzene (DAB; Vector Laboratories) was used as the peroxidize substrate and counterstaining was with methyl green (Calbiochem, EMD Biosciences), after which specimens were mounted using Permount (Vector Laboratories).

QUANTITATIVE REVERSE TRANSCRIPTASE POLYMERASE CHAIN REACTION (QRT-PCR)

Total RNA was extracted from bones using TRIzol reagent, and 3 μg was treated with DNase I (Invitrogen) at 1 U of DNase I/μg of RNA then reverse transcribed using Maxima Reverse Transcriptase (Fermentas, Burlington, ON, Canada) according to the manufacturer's instructions. qRT-PCR was performed using BioRad iQ SYBR Green Supermix in a Mx3000P qPCR system (Stratagene, Hercules, CA). Primer sequences used in the reactions were: *L32*, forward (5′–3′) *CACAATGTCAAGGAGCTGGAAGT*, reverse (5′–3′) *TCTACAATGGCTTTTCGGTTCT*, *a3*, forward (5′–3′) *CACCCGGGGGCCACATTCAG*, reverse (5′–3′) *CCCTCGCGGCACACCAGACC*, *Trap*, forward (5′–3′) *ACACAGTGATGCTGTGTGGCAACTC*, reverse (5′–3′) *CCAGAGGCTTCCACATATATGATGG*. Conventional PCR reactions were performed in 50 μl volumes using HotStarTaq polymerase (Qiagen, Valencia, CA). PCR products were visualized using GeneSnap software version 4.00.00 (SynGene, Cambridge, UK). The primer sequence used in the reaction was: a2 forward (5′–3′) *GGCCAGTCCTCCCGCACCAC*, reverse (5′–3′) *GCCCGCCACAGCATCCTTTCA*. All qRT-PCR data were normalized to the ribosomal protein L32. All conventional PCR data were normalized to *Gapdh*. Three separate experiments were performed, each on four 1-day-old mice per genotype.

PROTEIN ISOLATION FROM BONES

Femurs and tibias from newborn mice were excised and cleaned of soft tissue, snap frozen in liquid nitrogen then crushed under liquid nitrogen with a mortar and pestle. The resulting bone powder was incubated overnight with gentle shaking at 4°C in lysis buffer containing 50 mM Tris pH 8.0, 150 mM NaCl, 2 mM EDTA, 1% Triton X-100, 1% SDS, 0.5% sodium deoxycholate, 1 mM PMSF, and protease inhibitor cocktail from Sigma (Oakville, ON, Canada; P8340). The sample was centrifuged at 12,000*g* for 20 min at 4°C and protein concentrations were measured by the bicinchoninic acid (BCA) protein assay (Pierce, Nepean, ON, Canada).

IMMUNOBLOTTING

Sixty micrograms of protein isolated from bones (as described above) was separated by 10% SDS–PAGE, transferred to nitrocellulose membrane, and probed for V-ATPase subunit a3 (rabbit polyclonal antibody described above) and E (from Dr. Beth Lee, Ohio State University, OH), LC3 (polyclonal antibody, Thermo Scientific, Rockford, IL), SQSTM1/p62 (polyclonal antibody, Abcam), and GAPDH antibody (Abcam). Images were captured using BioRad ChemiDoc Gel Docking System and Quantity One software (BioRad, Hercules, CA) and analyzed by rolling disk method using Quantity One software.

OSTEOCLAST ISOLATION FROM SPLEEN

Splenocytes from P3 mice were plated at a cell density of 1×10^6 cells/ml on a Corning Osteo Assay Surface (Corning Life Sciences, Tewksbury, MA) in 10% fetal bovine serum, alpha MEM, and antibiotic (10 μg/ml penicillin G, 50 μg/ml gentamycin, 0.03 μg/ml fungizone) supplemented with 200 ng/ml soluble RANKL (made in-house) and 50 ng/ml M-CSF (Calbiochem) for 2 days, then media was replenished for another 3 days at 37°C and 5% CO_2.

ACRIDINE ORANGE STAINING

Spleen-derived osteoclasts were generated as above. On the 6th day of culture, the medium was changed for alpha MEM including 10% FBS and acridine orange at 5 μg/ml (Invitrogen) for 15 min at 37°C, washed with warm PBS (37°C) and chased for 10 min in alpha MEM plus 10% FBS without acridine orange. Acid production was observed under a Leica DM IRE2 microscope (Wetzlar, Germany) with a 490 nm excitation filter and a 525-nm emission filter in the presence and absence of 100 ng/ml concanamycin.

STATISTICAL ANALYSIS

Results are presented as mean ± s.d.; n value is defined in table and figure legends. Statistical analysis was performed using an unpaired two-tailed Student's *t*-test, and *P* values are included with all results.

RESULTS

R740S/R740S MICE APPEAR NORMAL AT BIRTH BUT DIE BY POSTNATAL DAY 14

R740S/R740S mice are born at the Mendelian ratio and are indistinguishable at birth from their +/+ littermates. Histopathology confirms normal development of all organ systems in newborn R740S/R740S mice (data not shown). However, by P14, mutant mice are smaller, have a significantly decreased body weight compared to +/+ mice (6.03 ± 0.29 g vs. 10.9 ± 1.1 g, respectively) and exhibit a malformed dome-shaped skull (Fig. 1A). At P13–14, R740S/R740S mice are unable to right themselves during a rotarod test and display unsteady gait and some circling behavior, possibly as a result of compression of the midbrain (hippocampus) secondary to defective skull development seen by histopathology. Like *oc*/*oc* mice [Schinke et al., 2009], R740S/R740S mice exhibit features of osteopetrorickets,

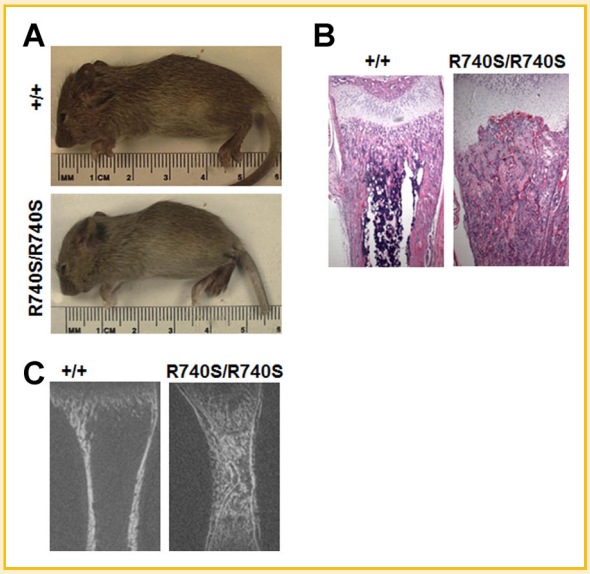

Fig. 1. a3 R740S/R740S mice appear normal at birth but die by postnatal day 14. A: Appearance of R740S/R740S mice at day 14. The R740S/R740S mouse is smaller and exhibits a domed head and shortened face. B: H&E stained images of femurs from P14 mice show the disorganized growth plate, widened metaphysis and irregular trabeculae in R740S/R740S femur. C: Micro-CT images from P5 mice reveal excessive trabecular bone in R740S/R740S femur.

including a disorganized growth plate, widened metaphysis, and irregular trabeculae (primary spongiosa) that contain a central cartilaginous core surrounded by variably thick layers of osteoid and mineralized bone (Fig. 1B).

No difference in osteoblast surface/bone surface (Ob.S/BS) is observed, but large increases in both the number of osteoclasts (Oc.N) and osteoclast surface/bone surface (Oc.S/BS) are seen in R740S/R740S compared to +/+ P1 femurs (summarized in Table I). Micro-CT analysis indicates that P5 R740S/R740S mice display a severe osteopetrotic phenotype as demonstrated by a dramatic increase in bone volume (BV/TV), trabecular number (Tb.N), bone mineral density (BMD), and bone mineral content (BMC), and significant decrease of trabecular spaces (Tb.S) and bone marrow area (Fig. 1C, Table I). Serum analysis reveals that calcium, phosphorous, and glucose levels are significantly decreased in R740S/R740S versus +/+ mice (Table I); the decreased glucose in serum has not been reported in other a3 mutant mouse models, however, the glucose result is consistent with the observation of emaciation that occurs prior to death.

TABLE I. Analysis of R740S/R740S and Wild-Type Femurs Using μCT and Histomorphometric Analyses

	+/+	R740S/R740S	*P*-value
μCT imaging			
BMC (mg)	0.0971 ± 0.005	1.21 ± 0.014*	0.010
BMD (mg/cm^3)	150 ± 7.37	192 ± 8.77*	0.007
BV/TV (%)	25.1 ± 10.3	42.3 ± 11.1*	0.001
Marrow area (mm^2)	0.32 ± 0.013	0.033 ± 0.022*	0.007
Tb.N	7.93 ± 0.52	17.8 ± 1.54*	0.006
Tb.S (μm)	0.11 ± 0.003	0.042 ± 0.006*	0.004
Tb.Th (μm)	0.0332 ± 0.002	0.025 ± 0.003*	0.002
Histomorphometry			
Ob.S/BS (%)	16.6 ± 4.34	16.5 ± 5.12	0.594
N.Oc	56.6 ± 13.2	91.4 ± 8.53*	0.016
Oc.S/BS (%)	7.93 ± 1.16	13.7 ± 3.15*	0.043
Serum (P10)			
Calcium (mmol/L)	2.54 ± 0.242	1.90 ± 0.294*	0.040
Phosphorous (mmol/L)	6.01 ± 0.223	3.63 ± 0.84*	0.022
Glucose (mmol/L)	5.92 ± 0.165	4.34 ± 0.19*	0.008

Femurs from 5-day-old mice were analyzed by μCT (n = 4/genotype). Femurs from P1 mice (n = 5/genotype) were analyzed for static histomorphometric parameters. Sera from P10 mice (n = 5/genotype) were analyzed. *$P = 0.05$.
BMC, bone mineral content; BMD, bone mineral density; BV/TV, bone volume/tissue volume; Tb.N, trabecular number; Tb.S, trabecular space; Tb.Th, trabecular thickness; Ob.S/BS, osteoblast surface/bone surface; Oc.S/BS, osteoclast surface/bone surface; N.Oc, number of osteoclasts.

These results demonstrate that even though R740S/R740S mice exhibit no detectable phenotype at birth, they develop severe osteopetrosis and die by P14. Therefore, to elucidate the specific effects of the mutation and to avoid the secondary effects of emaciation and other physiological changes that occur before death, all subsequent experiments were conducted using mice between P1 and P4.

R740S/R740S OSTEOCLASTS EXPRESS NORMAL LEVELS OF A3 BUT IT IS MISLOCALIZED

Quantitative PCR (qPCR) analysis demonstrates that a3 mRNA is expressed in mutant bones, although the levels are decreased (~10%) in R740S/R740S compared to +/+ bones (Fig. 2A). Despite the decrease in expression of a3 mRNA, the mRNA expression level of a2 is similar in R740S/R740S and +/+ bones (Fig. 2B, C). Protein levels of a3 are not significantly different between the genotypes (Fig. 3A,B) and protein levels of subunit E, an ubiquitous V_1 subunit, are also similar between the genotypes (Fig. 3A,C) suggesting that the R470S mutation does not affect protein expression of either V_1 (E) or V_0 (a3)

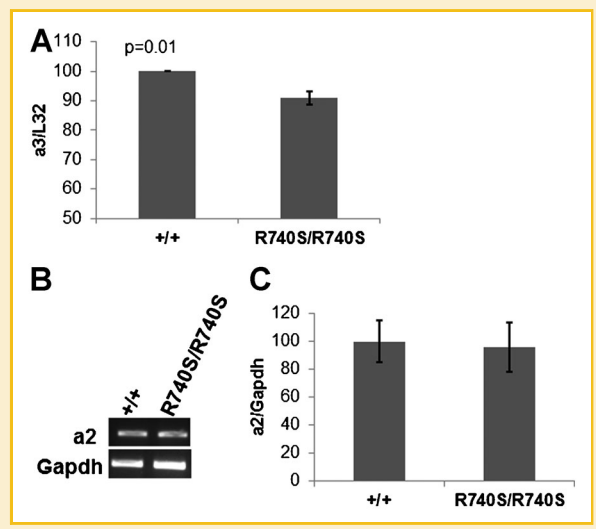

Fig. 2. Small decrease in a3 mRNA expression but no difference in mRNA expression of a2. A: Real-time PCR analysis of a3 mRNA expression in long bones of P1 R740S/R740S mice reveal a small yet significant (10%) decrease in a3 expression ($P = 0.01$). Values are the average ± 1 SD of four mice normalized to housekeeping gene L32 and expressed as the percentage of +/+ levels. B: Conventional PCR shows that R740S/R740S bones contain a similar level of a2 mRNA as +/+ bones. C: Quantification of expression of a2, normalized to *Gapdh* and the ratio of the bones were set at 100%.

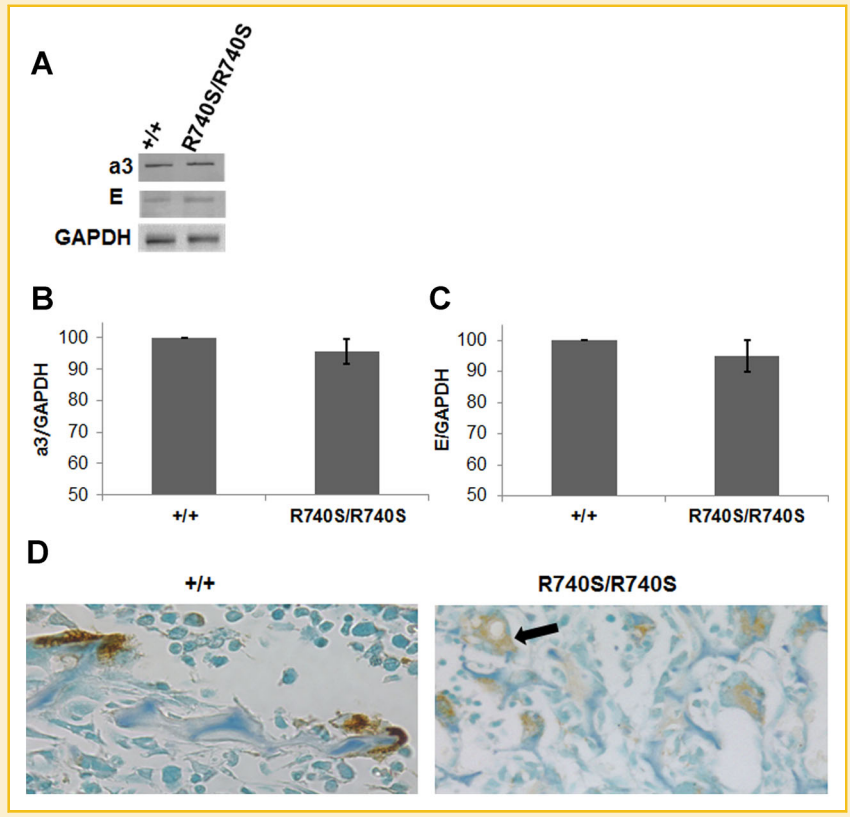

Fig. 3. R740S/R740S osteoclasts express normal levels of a3 but it is mislocalized. A: Representative immunoblots of whole bone protein lysates (60 μg) show equivalent expression of the V-ATPase V_0 subunit a3 and V_1 subunit E in R740S/R740S relative to +/+ long bone. B, C: The a3 and E proteins were each normalized to GAPDH and the ratios of +/+ bone protein were set at 100% (n = 5 mice/genotype). D: Diffuse a3 staining in R740S/R740S osteoclasts. Representative images of +/+ and R740S/R740S bones stained for the a3 subunit of V-ATPase at 20× magnification. The arrow points to an osteoclast containing a large vesicle (n = 12/genotype)

domain subunits. However, whereas immunohistochemistry confirms that a3 protein is expressed predominantly in osteoclasts in both genotypes, its distribution varies greatly between +/+ and R740S/R740S cells. a3 staining is more intense and localized primarily at the ventral side (adjacent to the bone surface) in +/+ osteoclasts, while the staining is fainter and evenly distributed throughout the cytoplasm in R740S/R740S osteoclasts (Fig. 3D).

R740S/R740S OSTEOCLASTS HAVE INCREASED APOPTOSIS AND ACIDIFICATION OF EXTRACELLULAR AND INTRACELLULAR COMPARTMENTS DOES NOT OCCUR

TUNEL staining reveals increased osteoclast apoptosis in long bones from R740S/R740S compared with +/+ mice (Fig. 4A); however, there is no difference in osteoblast and osteocyte apoptosis between the genotypes (osteoblasts: 3% vs. 2% apoptosis; osteocytes: 2% vs. 2% apoptosis, R740S/R740S vs. +/+, respectively). Increased osteoclast apoptosis is an unexpected finding considering that the number of osteoclasts is increased in R740S/R740S bones. An assay with splenocyte-derived osteoclasts reveals that resorption by R740S/R740S osteoclasts is virtually undetectable (Fig. 4B). Acridine orange (a lysosomal dye that stains acidic compartments) reveals that +/+ osteoclasts have a strong fluorescent staining of intracellular compartments as expected, while R740S/R740S osteoclasts display minimal staining, indicating absence of acidification (Fig. 4C). Taken together, these results indicate that the R740S mutation disrupts both intracellular and extracellular acidification in osteoclasts.

R740S/R740S OSTEOCLASTS EXHIBIT ABNORMAL MORPHOLOGY

Closer investigation of the osteoclasts within the long bones of R740S/R740S mice reveals that TRAP localization, similarly to that of a3, is also different between the genotypes, with +/+ osteoclasts exhibiting intense TRAP staining mostly at the ventral side adjacent to the bone surface, but relatively homogeneous staining in R740S/R740S osteoclasts (Fig. 5A). In addition, large cytoplasmic vacuoles are evident in R740S/R740S but not +/+ osteoclasts (these vacuoles can also be seen in R740S/R740S osteoclasts stained for a3; Fig. 3D). Transmission electron microscopy (TEM) reveals that osteoclasts from R740S/R740S mice have no ruffled borders, no polarization and numerous vacuoles (Fig. 5B). These results indicate that R740S/R740S osteoclasts not only have impaired function, but also display aberrant morphology.

a3 R740S/R740S OSTEOCLASTS HAVE FEWER AUTOPHAGOSOMES DUE TO DEFECTIVE EARLY STAGE AUTOPHAGY

Several studies have shown that inhibiting V-ATPase activity with bafilomycin A1 induces the formation of large numbers of autophagosomes [Hsin et al., 2012]. We therefore predicted that

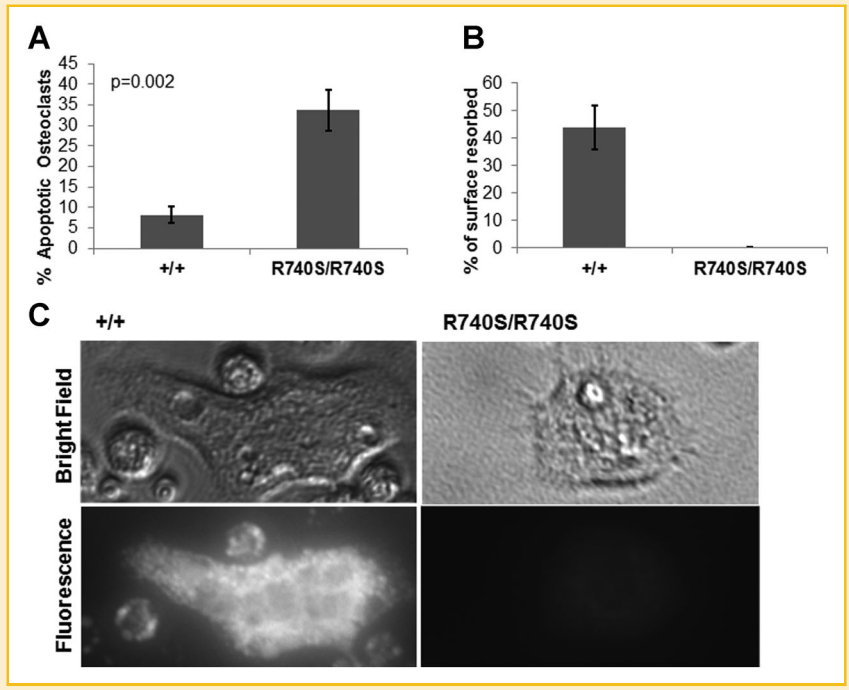

Fig. 4. a3 R740S/R740S osteoclasts have increased apoptosis and acidification of extracellular and intracellular compartments does not occur. A: Increased apoptosis of R740S/R740S osteoclasts ($P = 0.002$). TUNEL assay was conducted on long bone sections (n = 10/genotype). B: Resorption assay on Corning Osteo Assay surface. The surface was not resorbed by R740S/R740S osteoclasts. n = 4 per genotype plated in triplicate. C: Acidic compartments were detected in +/+ cells but not R740S/R740S cells grown on Corning Osteo Assay surfaces. The upper images are representative brightfield pictures of osteoclasts and the lower images are fluorescent pictures of the same cells, 40× magnification; n = 4 per genotype plated in triplicate.

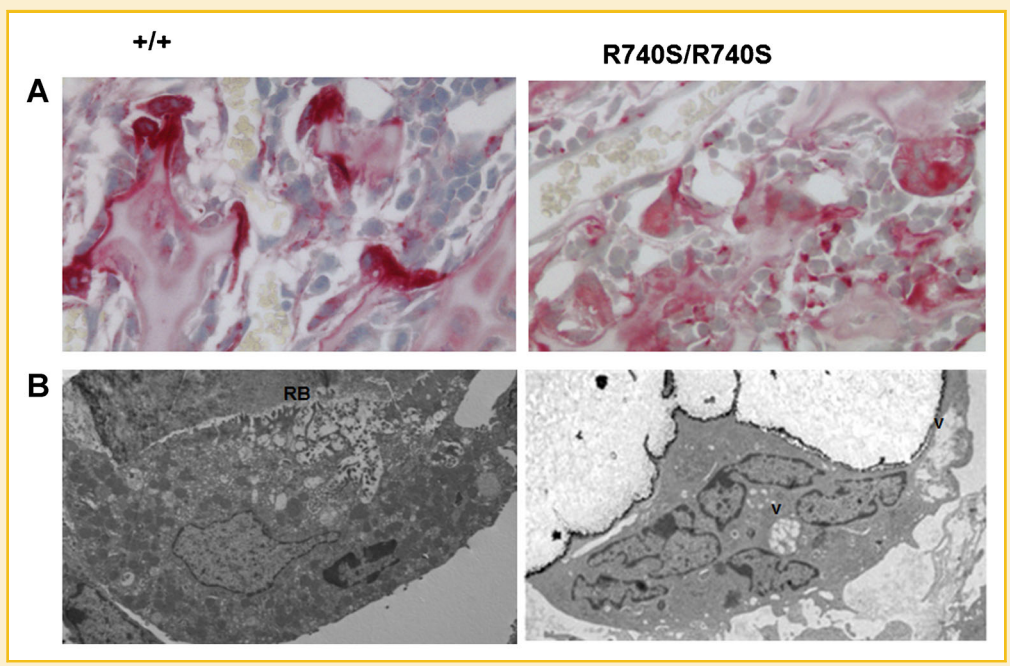

Fig. 5. a3 R740S/R740S osteoclasts have abnormal morphology. A: Diffuse TRAP localization in R740S/R740S osteoclasts. Representative images of +/+ (upper left) and R740S/R740S (upper right) bone sections stained for TRAP at 20× magnification. B: Representative transmission electron micrographs from the lower metaphyseal region of femurs +/+ (lower right) and R740S/R740S (lower left). R740S/R740S osteoclasts lack polarization, ruffled borders, and contain numerous vesicles. (n = 4/genotype; RB, ruffled border, V, vesicles).

the accumulated vesicles within R740S/R740S osteoclasts are autophagosomes. However, when the number of autophagosomes, defined as double membrane structures surrounding cytoplasmic contents (depicted in Fig. 6A), was quantified, we found fewer autophagosomes within R740S/R740S compared to +/+ osteoclasts (Fig. 6B). To assess autophagic flux we looked at two well-known proteins used to monitor autophagy, microtubule-associated protein 1 light chain 3 (LC3), a marker for autophagosomes and sequestosome 1/SQSTM1 (p62), a protein degraded primarily by autophagy [Bjorkoy et al., 2005; Klionsky et al., 2008]. LC3 exists in two forms; LC3I is diffusely localized in the cytoplasm while LC3 II is associated with autophagosomes [Mizushima et al., 2010]. Consistent with a block in autophagosome formation, the autophagosome-associated LC3II protein levels are decreased while the level of LC3I is unchanged in R740S/R740S compared with +/+ long bone protein lysates (Fig. 7A,B). LC3 staining within +/+ osteoclasts is more punctuate as expected, while the staining within R740S/R740S osteoclasts is less punctuated (Fig. 8A). Immunoblotting of long bone protein lysates reveals an accumulation of p62 in R740S/R740S long bone protein lysates relative to +/+ (Fig. 7A,C) and p62 staining is darker and more punctate within R740S/R740S osteoclasts compared to +/+ osteoclasts (8B). The low LC3II expression and accumulation of p62 are consistent with an early stage defect in autophagy [Mizushima and Yoshimori, 2007].

DISCUSSION

In this study, we provide novel insights into the role of V-ATPases in osteoclast maturation, function and autophagy using the osteopetrotic a3 R740S/R740S mutant mouse model. Similarly to other mutants with loss-of-function of the a3 subunit, that is, the *oc*/*oc* and *Tcirg1*$^{-/-}$ mouse models [Marks et al., 1985; Li et al., 1999], homozygous a3 R740S/R740S mice develop progressive osteopetrosis and die at a young age due to the severity of the disease. Also consistent with the osteopetrotic phenotype observed in humans and mouse models [Udagawa et al., 1992; Taranta et al., 2003; Neutzsky-Wulff et al., 2010], the R740S/R740S osteoclasts lack polarization and have no ruffled border. However, R740S/R740S osteoclasts also exhibit unique features such as no intracellular acidification, increased apoptosis, diffuse localization of the a3 protein and defective early stage autophagy.

The lack of intracellular acidification, which contrasts with what is seen in osteoclasts from +/R740S, *oc*/*oc* and *Tcirg1*$^{-/-}$ mice [Marks et al., 1985; Li et al., 1999; Voronov et al., 2013], likely accounts for the aberrant localization of TRAP and a3 itself, as well as the lack of polarization of R740S/R740S osteoclasts. Acidification of lysosomes in +/R740S osteoclasts presumably reflects the residual activity from a wild-type copy of the a3 subunit. Acidification of lysosomes in *oc*/*oc* and *Tcirg1*$^{-/-}$ osteoclasts likely reflects from the high

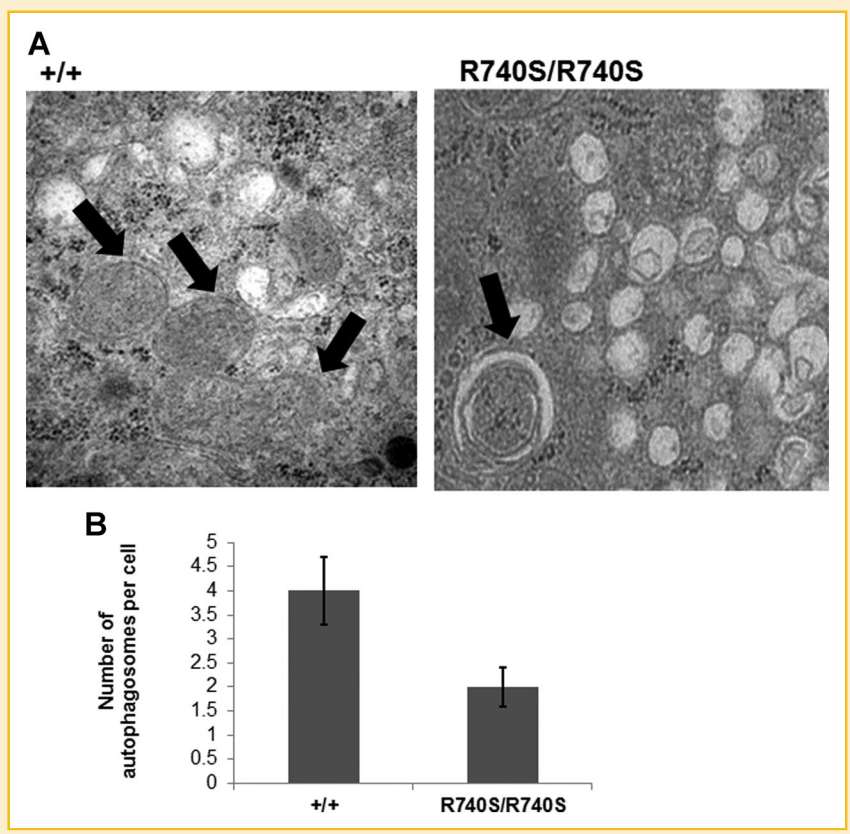

Fig. 6. a3 R740S/R740S osteoclasts have fewer autophagosomes. A: Representative transmission electron micrograph images depicting the vesicular structures found within the +/+ and R740S/R740S osteoclasts. Arrows point to autophagosomes defined as double membrane structures that contain cytoplasmic contents. B: R740S/R740S osteoclasts contain fewer autophagosomes ($P = 0.003$; n = 7 osteoclasts/genotype).

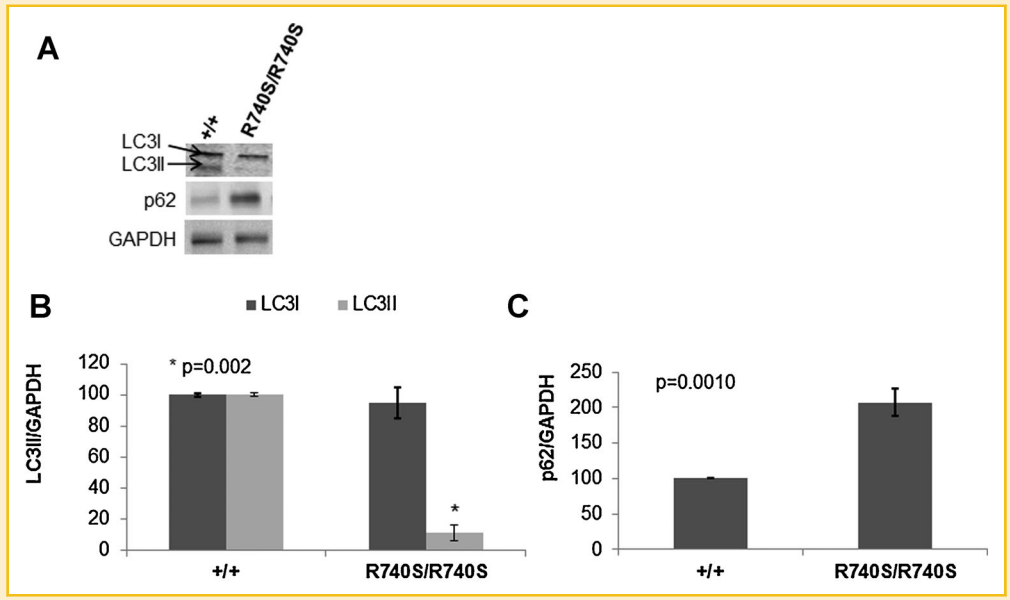

Fig. 7. R740S/R740S osteoclasts express decreased LC3II and increased p62 and show defective early stage autophagy. A: Representative immunoblots of whole bone protein lysates (60 μg) shows reduced expression of LC3II ($P = 0.002$) and increased expression of p62 ($P = 0.001$) in R740S/R740S relative to +/+ bones (n = 5/genotype). B, C: Quantification of LC3II and p62 protein. The LC3II and p62 proteins were each normalized to GAPDH and the ratios of +/+ bone protein were set at 100%.

compensatory expression of the a2 isoform in the complete absence of a3 [Sun-Wada et al., 2006], a compensation that is not seen with the homozygous expression of a3 R740S within R740S/R740S osteoclasts.

A variety of data support the view that lack of intracellular acidification prevents the polarized trafficking, targeting and fusion of acidified vesicles such as lysosomes with the plasma membrane to form the ruffled border [Palokangas et al., 1997; Mulari et al., 2003;

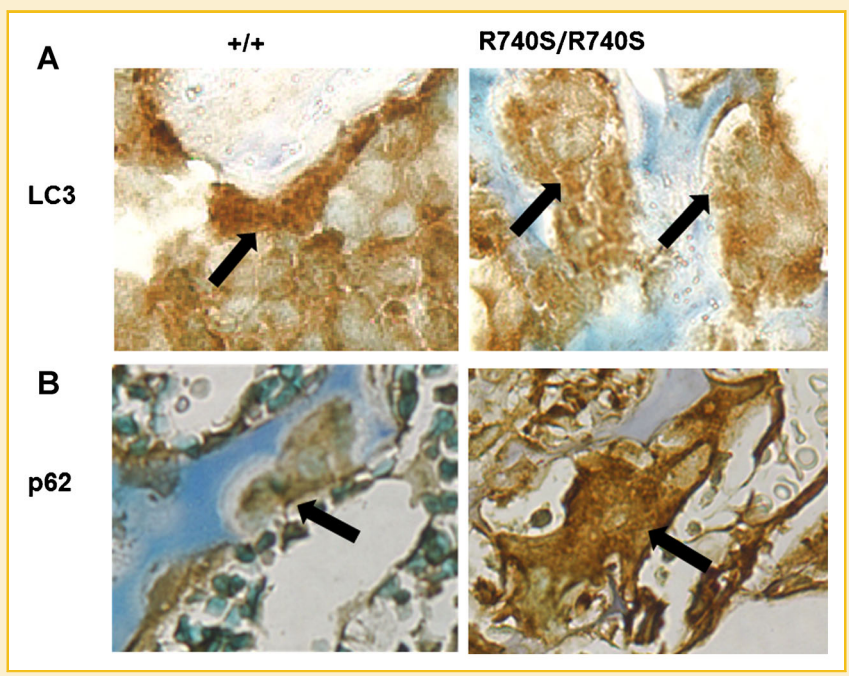

Fig. 8. Diffuse staining of LC3 and darker staining of p62 in R740S/R740S osteoclasts reveals defective autophagy. A: Diffuse staining of LC3 in R740S/R740S osteoclasts in long bone (n = 9, +/+ and n = 10, R740S/R470S), 40× magnification. Arrows indicate osteoclasts. B: Darker punctate staining of p62 in R740S/R740S osteoclasts in long bone (n = 9, +/+ and n = 10, R740S/R470S), 40× magnification. Arrows point to the osteoclasts.

Yang et al., 2012]. LC3II and a3-containing V-ATPases are found within acidified vesicles and at the ruffled border of osteoclasts [DeSelm et al., 2011; Chung et al., 2012]. Similarly to R740S/R740S osteoclasts, osteoclasts from mice lacking *Trap* or *Plekhm1* contain numerous large vesicles throughout the cytoplasm, which are thought to reflect defective trafficking within the cell [Hollberg et al., 2002; Van Wesenbeeck et al., 2007]. Additionally, osteoclasts from a patient with a point mutation in *PLEKHM1* have reduced endosome/lysosome acidification [Del Fattore et al., 2008] and lack ruffled borders [Van Wesenbeeck et al., 2007]. Moreover, silencing the V-ATPase accessory subunit Ac45 results in reduced intracellular acidification and reduced endocytosis, which is attributed to defective trafficking of lysosomes and endosomes within the osteoclasts, concomitant with lack of polarization and lack of bone resorption [Qin et al., 2011].

The lack of intracellular acidification may also account for the increased apoptosis seen in R740S/R740S long bone osteoclasts in vivo, which was not seen in R740S/R740S osteoblasts and osteocytes or +/R740S osteoclasts in vivo [Ochotny et al., 2011]. Osteoclasts are 100-fold enriched for a3 [Manolson et al., 2003] so are more sensitive to disruption of V-ATPase activity compared with other cells. This is consistent with the observation that treatment with inhibitors of V-ATPase activity, such as bafilomycin A1 or concanamycin A, results in osteoclast apoptosis specifically, without affecting osteoblasts [Okahashi et al., 1997; Xu et al., 2003].

R740S/R740S osteoclasts, exhibit fewer autophagosomes, have low LC3II expression and an accumulation of p62, all of which are consistent with an early stage defect in autophagy [Yamamoto et al., 1998; Bjorkoy et al., 2005; Mizushima and Yoshimori, 2007; Hsin et al., 2012]. In studies with *Drosophila* neurons, the loss of the a1 subunit of V-ATPases results in defective endosomal/lysosomal acidification and inhibition of autophagy, resulting in increased susceptibility to neurotoxic insults [Williamson and Hiesinger, 2010]. It is thus interesting to speculate that the lack of acidification of internal compartments may result in increased sensitivity of R740S/R740S osteoclasts to toxic events such as accumulated misfolded proteins that would normally be removed by the autophagy process, resulting in apoptosis. In this regard, it is also notable that p62 is involved not only in autophagy, but can interact with both TRAF 6 to stimulate osteoclastogenesis and with caspace 8 to promote apoptosis [McManus and Roux, 2012]. Whether and how the excess p62 detected within R740S/R740S osteoclasts directly affects the balance between osteoclastogenesis and apoptosis remains to be explored further.

Growing evidence supports multifunctional roles for not only p62 but also for other proteins involved in autophagy. In osteoclasts, the formation of a ruffled border requires LC3 and other autophagy proteins such as Atg4B, Atg5, and Atg7 [DeSelm et al., 2011]. Indeed, conversion of LC3I to LC3II is correlated with osteoclast maturation and function [DeSelm et al., 2011; Chung et al., 2012] and increased conversion of LC3I to LC3II is correlated with osteoclast resorptive activity but not autophagic activity [DeSelm et al., 2011; Chung et al., 2012]. Similarly, an in vitro LC3 knockdown study reveals no effect on osteoclast differentiation but mature osteoclast functions such as cathepsin K release and actin ring formation, and therefore bone resorption, are reduced [Chung et al., 2012]. Over expression of Beclin 1, an autophagy protein enhances both osteoclastogenesis and resorptive capacity of osteoclasts, while pharmacological inactivation of autophagy prevents osteoclast differentiation [Lin et al., 2012]. These studies taken together provide evidence that autophagy proteins are involved in osteoclastogenesis, maturation, and function. The aberrant levels of LC3 conversion and p62 in R740S/R740S osteoclasts correlates with their lack of ruffled borders and other anomalies, and supports the need for additional studies to dissect the functional inter-relationships of autophagy proteins and other aspects of osteoclast maturation.

In summary, our observations on R740S/R740S mice and osteoclasts indicate the importance of intracellular acidification for the early stages of autophagy as well as for osteoclast survival, maturation, and for the appropriate cytoplasmic distribution of key osteoclast enzymes such as TRAP and ruffled border formation.

ACKNOWLEDGMENTS

We thank the following for their contributions to this work: H. Adissu (Centre for Modeling Human Disease) for conducting histopathology; Dr. Beth S. Lee (Department of Physiology and Cell Biology, Ohio State University College of Medicine, Columbus, OH) for providing anti-E antibody; members of the Aubin Lab for assistance with dissection and helpful discussion; K. Lee (Manolson Lab) for making the recombinant soluble RANKL; F. Serraf at the Dental Research Institute Histology Lab for paraffin embedding, cutting, and TRAP staining femur sections, and N. Kartner for helpful discussion.

REFERENCES

Bjorkoy G, Lamark T, Brech A, Outzen H, Perander M, Overvatn A, Stenmark H, Johansen T. 2005. p62/SQSTM1 forms protein aggregates degraded by autophagy and has a protective effect on huntingtin-induced cell death. J Cell Biol 171:603–614.

Chalhoub N, Benachenhou N, Rajapurohitam V, Pata M, Ferron M, Frattini A, Villa A, Vacher J. 2003. Grey-lethal mutation induces severe malignant autosomal recessive osteopetrosis in mouse and human. Nat Med 9:399–406.

Chung YH, Yoon SY, Choi B, Sohn DH, Yoon KH, Kim WJ, Kim DH, Chang EJ. 2012. Microtubule-associated protein light chain 3 regulates Cdc42-dependent actin ring formation in osteoclast. Int J Biochem Cell Biol 44:989–997.

Del Fattore A, Fornari R, Van Wesenbeeck L, de Freitas F, Timmermans JP, Peruzzi B, Cappariello A, Rucci N, Spera G, Helfrich MH, Van Hul W, Migliaccio S, Teti A. 2008. A new heterozygous mutation (R714C) of the osteopetrosis gene, pleckstrin homolog domain containing family M (with run domain) member 1 (PLEKHM1), impairs vesicular acidification and increases TRACP secretion in osteoclasts. J Bone Miner Res 23:380–391.

DeSelm CJ, Miller BC, Zou W, Beatty WL, van Meel E, Takahata Y, Klumperman J, Tooze SA, Teitelbaum SL, Virgin HW. 2011. Autophagy proteins regulate the secretory component of osteoclastic bone resorption. Dev Cell 21:966–974.

Fasth A, Porras O. 1999. Human malignant osteopetrosis: Pathophysiology, management and the role of bone marrow transplantation. Pediatr Transplant 1(3Suppl):102–107.

Frattini A, Orchard PJ, Sobacchi C, Giliani S, Abinun M, Mattsson JP, Keeling DJ, Andersson AK, Wallbrandt P, Zecca L, Notarangelo LD, Vezzoni P, Villa A. 2000. Defects in TCIRG1 subunit of the vacuolar proton pump are responsible

for a subset of human autosomal recessive osteopetrosis. Nat Genet 25: 343–346.

Frattini A, Pangrazio A, Susani L, Sobacchi C, Mirolo M, Abinun M, Andolina M, Flanagan A, Horwitz EM, Mihci E, Notarangelo LD, Ramenghi U, Teti A, Van Hove J, Vujic D, Young T, Albertini A, Orchard PJ, Vezzoni P, Villa A. 2003. Chloride channel ClCN7 mutations are responsible for severe recessive, dominant, and intermediate osteopetrosis. J Bone Miner Res 18:1740–1747.

Gerritsen EJ, Vossen JM, Fasth A, Friedrich W, Morgan G, Padmos A, Vellodi A, Porras O, O'Meara A, Porta F, et al. 1994. Bone marrow transplantation for autosomal recessive osteopetrosis. A report from the Working Party on Inborn Errors of the European Bone Marrow Transplantation Group. J Pediatr 125:896–902.

Hollberg K, Hultenby K, Hayman A, Cox T, Andersson G. 2002. Osteoclasts from mice deficient in tartrate-resistant acid phosphatase have altered ruffled borders and disturbed intracellular vesicular transport. Exp Cell Res 279:227–238.

Hsin IL, Sheu GT, Jan MS, Sun HL, Wu TC, Chiu LY, Lue KH, Ko JL. 2012. Inhibition of lysosome degradation on autophagosome formation and responses to GMI, an immunomodulatory protein from Ganoderma microsporum. Br J Pharmacol 167(6):1287–1300.

Kawasaki-Nishi S, Nishi T, Forgac M. 2001. Arg-735 of the 100-kDa subunit a of the yeast V-ATPase is essential for proton translocation. Proc Natl Acad Sci USA 98:12397–12402.

Kawasaki-Nishi S, Nishi T, Forgac M. 2003. Interacting helical surfaces of the transmembrane segments of subunits a and c′ of the yeast V-ATPase defined by disulfide-mediated cross-linking. J Biol Chem 278:41908–41913.

Klionsky DJ, Abeliovich H, Agostinis P, Agrawal DK, Aliev G, Askew DS, Baba M, Baehrecke EH, Bahr BA, Ballabio A, Bamber BA, Bassham DC, Bergamini E, Bi X, Biard-Piechaczyk M, Blum JS, Bredesen DE, Brodsky JL, Brumell JH, Brunk UT, Bursch W, Camougrand N, Cebollero E, Cecconi F, Chen Y, Chin LS, Choi A, Chu CT, Chung J, Clarke PG, Clark RS, Clarke SG, Clave C, Cleveland JL, Codogno P, Colombo MI, Coto-Montes A, Cregg JM, Cuervo AM, Debnath J, Demarchi F, Dennis PB, Dennis PA, Deretic V, Devenish RJ, Di Sano F, Dice JF, Difiglia M, Dinesh-Kumar S, Distelhorst CW, Djavaheri-Mergny M, Dorsey FC, Droge W, Dron M, Dunn WA Jr, Duszenko M, Eissa NT, Elazar Z, Esclatine A, Eskelinen EL, Fesus L, Finley KD, Fuentes JM, Fueyo J, Fujisaki K, Galliot B, Gao FB, Gewirtz DA, Gibson SB, Gohla A, Goldberg AL, Gonzalez R, Gonzalez-Estevez C, Gorski S, Gottlieb RA, Haussinger D, He YW, Heidenreich K, Hill JA, Hoyer-Hansen M, Hu X, Huang WP, Iwasaki A, Jaattela M, Jackson WT, Jiang X, Jin S, Johansen T, Jung JU, Kadowaki M, Kang C, Kelekar A, Kessel DH, Kiel JA, Kim HP, Kimchi A, Kinsella TJ, Kiselyov K, Kitamoto K, Knecht E, Komatsu M, Kominami E, Kondo S, Kovacs AL, Kroemer G, Kuan CY, Kumar R, Kundu M, Landry J, Laporte M, Le W, Lei HY, Lenardo MJ, Levine B, Lieberman A, Lim KL, Lin FC, Liou W, Liu LF, Lopez-Berestein G, Lopez-Otin C, Lu B, Macleod KF, Malorni W, Martinet W, Matsuoka K, Mautner J, Meijer AJ, Melendez A, Michels P, Miotto G, Mistiaen WP, Mizushima N, Mograbi B, Monastyrska I, Moore MN, Moreira PI, Moriyasu Y, Motyl T, Munz C, Murphy LO, Naqvi NI, Neufeld TP, Nishino I, Nixon RA, Noda T, Nurnberg B, Ogawa M, Oleinick NL, Olsen LJ, Ozpolat B, Paglin S, Palmer GE, Papassideri I, Parkes M, Perlmutter DH, Perry G, Piacentini M, Pinkas-Kramarski R, Prescott M, Proikas-Cezanne T, Raben N, Rami A, Reggiori F, Rohrer B, Rubinsztein DC, Ryan KM, Sadoshima J, Sakagami H, Sakai Y, Sandri M, Sasakawa C, Sass M, Schneider C, Seglen PO, Seleverstov O, Settleman J, Shacka JJ, Shapiro IM, Sibirny A, Silva-Zacarin EC, Simon HU, Simone C, Simonsen A, Smith MA, Spanel-Borowski K, Srinivas V, Steeves M, Stenmark H, Stromhaug PE, Subauste CS, Sugimoto S, Sulzer D, Suzuki T, Swanson MS, Tabas I, Takeshita F, Talbot NJ, Talloczy Z, Tanaka K, Tanida I, Taylor GS, Taylor JP, Terman A, Tettamanti G, Thompson CB, Thumm M, Tolkovsky AM, Tooze SA, Truant R, Tumanovska LV, Uchiyama Y, Ueno T, Uzcategui NL, van der Klei I, Vaquero EC, Vellai T, Vogel MW, Wang HG, Webster P, Wiley JW, Xi Z, Xiao G, Yahalom J, Yang JM, Yap G, Yin XM, Yoshimori T, Yu L, Yue Z, Yuzaki M, Zabirnyk O, Zheng X, Zhu X, Deter RL. 2008. Guidelines for the use and interpretation of assays for monitoring autophagy in higher eukaryotes. Autophagy 4:151–175.

Kornak U, Schulz A, Friedrich W, Uhlhaas S, Kremens B, Voit T, Hasan C, Bode U, Jentsch TJ, Kubisch C. 2000. Mutations in the a3 subunit of the vacuolar H(+)-ATPase cause infantile malignant osteopetrosis. Hum Mol Genet 9:2059–2063.

Kornak U, Kasper D, Bosl MR, Kaiser E, Schweizer M, Schulz A, Friedrich W, Delling G, Jentsch TJ. 2001. Loss of the ClC-7 chloride channel leads to osteopetrosis in mice and man. Cell 104:205–215.

Li YP, Chen W, Liang Y, Li E, Stashenko P. 1999. Atp6i-deficient mice exhibit severe osteopetrosis due to loss of osteoclast-mediated extracellular acidification. Nat Genet 23:447–451.

Lin NY, Beyer C, Giessl A, Kireva T, Scholtysek C, Uderhardt S, Munoz LE, Dees C, Distler A, Wirtz S, Kronke G, Spencer B, Distler O, Schett G, Distler JH. 2012. Autophagy regulates TNFalpha-mediated joint destruction in experimental arthritis. Ann Rheum Dis 72:761–768.

Manolson MF, Yu H, Chen W, Yao Y, Li K, Lees RL, Heersche JN. 2003. The a3 isoform of the 100-kDa V-ATPase subunit is highly but differentially expressed in large (> or =10 nuclei) and small (< or = nuclei) osteoclasts. J Biol Chem 278:49271–49278.

Marks SCJ, Seifert MF, Lane PW. 1985. Osteosclerosis, a recessive skeletal mutation on chromosome 19 in the mouse. J Hered 76:171–176.

McManus S, Roux S. 2012. The adaptor protein p62/SQSTM1 in osteoclast signaling pathways. J Mol Signal 7:doi: 10.1186/1750-2187-7-1

Mizushima N, Yoshimori T. 2007. How to interpret LC3 immunoblotting. Autophagy 3:542–545.

Mizushima N, Yoshimori T, Levine B. 2010. Methods in mammalian autophagy research. Cell 140:313–326.

Mulari MT, Zhao H, Lakkakorpi PT, Vaananen HK. 2003. Osteoclast ruffled border has distinct subdomains for secretion and degraded matrix uptake. Traffic 4:113–125.

Neutzsky-Wulff AV, Sims NA, Supanchart C, Kornak U, Felsenberg D, Poulton IJ, Martin TJ, Karsdal MA, Henriksen K. 2010. Severe developmental bone phenotype in ClC-7 deficient mice. Dev Biol 334:1001–1010.

Nishi T, Forgac M. 2002. The vacuolar (H+)-ATPases–Nature's most versatile proton pumps. Nat Rev Mol Cell Biol 3:94–103.

Ochotny N, Flenniken AM, Owen C, Voronov I, Zirngibl RA, Osborne LR, Henderson JE, Adamson SL, Rossant J, Manolson MF, Aubin JE. 2011. The V-ATPase a3 subunit mutation R740S is dominant negative and results in osteopetrosis in mice. J Bone Miner Res 26:1484–1493.

Okahashi N, Nakamura I, Jimi E, Koide M, Suda T, Nishihara T. 1997. Specific inhibitors of vacuolar H(+)-ATPase trigger apoptotic cell death of osteoclasts. J Bone Miner Res 12:1116–1123.

Palokangas H, Mulari M, Vaananen HK. 1997. Endocytic pathway from the basal plasma membrane to the ruffled border membrane in bone-resorbing osteoclasts. J Cell Sci 110(Pt15):1767–1780.

Pietrement C, Sun-Wada GH, Silva ND, McKee M, Marshansky V, Brown D, Futai M, Breton S. 2006. Distinct expression patterns of different subunit isoforms of the V-ATPase in the rat epididymis. Biol Reprod 74: 185–194.

Qin A, Cheng TS, Lin Z, Pavlos NJ, Jiang Q, Xu J, Dai KR, Zheng MH. 2011. Versatile roles of V-ATPases accessory subunit Ac45 in osteoclast formation and function. PLoS ONE 6:e27155.

Schinke T, Schilling AF, Baranowsky A, Seitz S, Marshall RP, Linn T, Blaeker M, Huebner AK, Schulz A, Simon R, Gebauer M, Frattini A, Streichert T, Pueschel K, Villa A, Debatin KM, Rueger JM, Teti A, Zustin J, Sauter G, Amling M. 2009. Impaired gastric acidification negatively affects calcium homeostasis and bone mass. Nat Med 16:674–682.

Schlager G, Dickie MM. 1967. Spontaneous mutations and mutation rates in the house mouse. Genetics 57:319–330.

Sobacchi C, Frattini A, Orchard P, Porras O, Tezcan I, Andolina M, Babul-Hirji R, Baric I, Canham N, Chitayat D, Dupuis-Girod S, Ellis I, Etzioni A, Fasth A, Fisher A, Gerritsen B, Gulino V, Horwitz E, Klamroth V, Lanino E, Mirolo M, Musio A, Matthijs G, Nonomaya S, Notarangelo LD, Ochs HD, Superti Furga A, Valiaho J, van Hove JL, Vihinen M, Vujic D, Vezzoni P, Villa A. 2001. The mutational spectrum of human malignant autosomal recessive osteopetrosis. Hum Mol Genet 10:1767–1773.

Sun-Wada GH, Toyomura T, Murata Y, Yamamoto A, Futai M, Wada Y. 2006. The a3 isoform of V-ATPase regulates insulin secretion from pancreatic beta-cells. J Cell Sci 119:4531–4540.

Taranta A, Migliaccio S, Recchia I, Caniglia M, Luciani M, De Rossi G, Dionisi-Vici C, Pinto RM, Francalanci P, Boldrini R, Lanino E, Dini G, Morreale G, Ralston SH, Villa A, Vezzoni P, Del Principe D, Cassiani F, Palumbo G, Teti A. 2003. Genotype-phenotype relationship in human ATP6i-dependent autosomal recessive osteopetrosis. Am J Pathol 162:57–68.

Toei M, Saum R, Forgac M. 2010. Regulation and isoform function of the V-ATPases. Biochemistry 49:4715–4723.

Toyomura T, Murata Y, Yamamoto A, Oka T, Sun-Wada GH, Wada Y, Futai M. 2003. From lysosomes to the plasma membrane: Localization of vacuolar-type H+-ATPase with the a3 isoform during osteoclast differentiation. J Biol Chem 278:22023–22030.

Udagawa N, Sasaki T, Akatsu T, Takahashi N, Tanaka S, Tamura T, Tanaka H, Suda T. 1992. Lack of bone resorption in osteosclerotic (oc/oc) mice is due to a defect in osteoclast progenitors rather than the local microenvironment provided by osteoblastic cells. Biochem Biophys Res Commun 184: 67–72.

Van Wesenbeeck L, Odgren PR, Coxon FP, Frattini A, Moens P, Perdu B, MacKay CA, Van Hul E, Timmermans JP, Vanhoenacker F, Jacobs R, Peruzzi B, Teti A, Helfrich MH, Rogers MJ, Villa A, Van Hul W. 2007. Involvement of PLEKHM1 in osteoclastic vesicular transport and osteopetrosis in incisors absent rats and humans. J Clin Invest 117:919–930.

Voronov I, Ochotny N, Jaumouille V, Owen C, Manolson MF, Aubin JE. 2013. The R740S mutation in the V-ATPase a3 subunit increases lysosomal pH, impairs NFATc1 translocation, and decreases in vitro osteoclastogenesis. J Bone Miner Res 28:108–118.

Williamson WR, Hiesinger PR. 2010. On the role of v-ATPase V0a1-dependent degradation in Alzheimer disease. Commun Integr Biol 3:604–607.

Xu J, Feng HT, Wang C, Yip KH, Pavlos N, Papadimitriou JM, Wood D, Zheng MH. 2003. Effects of Bafilomycin A1: An inhibitor of vacuolar H (+)-ATPases on endocytosis and apoptosis in RAW cells and RAW cell-derived osteoclasts. J Cell Biochem 88:1256–1264.

Yamamoto A, Tagawa Y, Yoshimori T, Moriyama Y, Masaki R, Tashiro Y. 1998. Bafilomycin A1 prevents maturation of autophagic vacuoles by inhibiting fusion between autophagosomes and lysosomes in rat hepatoma cell line, H-4-II-E cells. Cell Struct Funct 23:33–42.

Yang DQ, Feng S, Chen W, Zhao H, Paulson C, Li YP. 2012. V-ATPase subunit ATP6AP1 (Ac45) regulates osteoclast differentiation, extracellular acidification, lysosomal trafficking, and protease exocytosis in osteoclast-mediated bone resorption. J Bone Miner Res 27:1695–1707.